Exploiting Rydberg Atom Surface Phonon Polariton Coupling for Single Photon Subtraction

H. Kübler,* D. Booth, J. Sedlacek, P. Zabawa, and J.P. Shaffer†
Homer L. Dodge Department of Physics and Astronomy, The University of Oklahoma, 440 W. Brooks St. Norman, OK 73019, USA
(Dated: April 29, 2013)

We investigate a hybrid quantum system that consists of a superatom coupled to a surface phonon-polariton. We apply this hybrid quantum system to subtract individual photons from a beam of light. Rydberg atom blockade is used to attain absorption of a single photon by an atomic microtrap. Surface phonon-polariton coupling to the superatom then triggers the transfer of the excitation to a storage state, a single Rydberg atom. The approach utilizes the interaction between a superatom and a Markovian bath that acts as a controlled decoherence mechanism to irreversibly project the superatom state into a single Rydberg atom state that can be read out.

PACS numbers: 42.50.Ct, 32.80.Ee, 42.50.Dv, 42.50.Ex, 32.80.Rm, 78.68.+m, 71.36.+c

Devices like quantum computers that rely on entanglement have proven difficult to realize and make robust. One school of thought suggests that advances require linking quantum sub-systems that are individually tailored to meet specific challenges presented by effects such as dephasing, readout and interfacing to conventional electronics, so called hybrid quantum systems [1]. Since the idea of an active device implies strong interactions and the idea of coherence weak interaction, at least with unwanted degrees of freedom, hybrid quantum systems that exploit particular quantum properties of different sub-systems to meet these seemingly contradictory criteria are a promising direction to pursue. Consequently, developing experiments and theory for the useful interfacing of disparate quantum objects like atoms and surfaces is increasingly important and interesting.

In this paper, we investigate a hybrid quantum system that consists of a superatom coupled to a surface phonon-polariton (SPP) [2], Figure 1. We apply this system to design a scheme for subtracting individual photons from a beam of light. Atom SPP coupling has been investigated previously in other contexts [3, 4]. We exploit the properties of a superatom and Rydberg atom blockade to limit absorption by an atomic microtrap to a single photon [5]. A superatom is a single Rydberg excitation coherently shared by a cluster of atoms contained in a volume determined by the Rydberg atom blockade radius, r_b [6–9]. After absorption, the excitation is stored by coupling the superatom to a SPP that quickly decays into the bulk polariton modes of a dielectric. The coupling between the superatom and the SPP is resonantly enhanced so that a specific Rydberg atom storage state can be populated. The decay to the storage state is irreversible and decoheres the superatom, which is important for detecting the photon subtraction and decoupling the excitation from the light fields. The excitation and transfer phases of the process benefit from the $\sqrt{N}$ enhancement of the transition amplitude supplied by the superatom state, where N is the number of atoms making up the superatom. In contrast, the storage state is a single excited Rydberg atom that decays at the rate of the populated Rydberg state. The dephasing of the superatom is accomplished via the decay into the SPP and Rydberg storage state since the correlations of the SPP Markovian bath die away much faster than the coherent dynamics present in the overall system, effectively performing a measurement on the superatom.

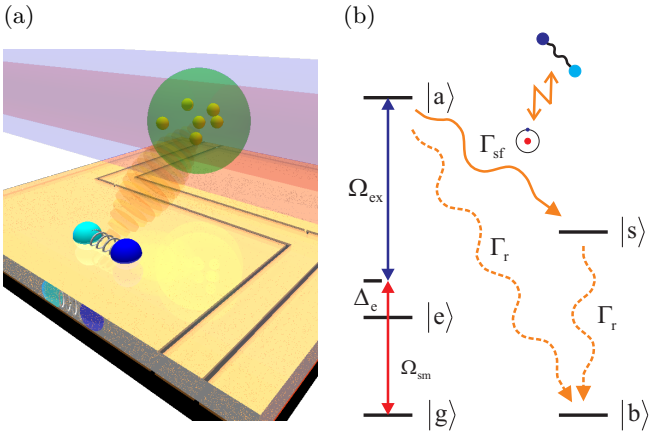

FIG. 1. (Color online) (a) Schematic view of photon subtraction and counting concept. Atoms are trapped above an atom chip. On top of the chip is a dielectric substrate. Laser beams parallel to the chip surface excite atoms into a superatom state. The decay of the superatom is resonantly enhanced by coupling to a SPP, shown in the foreground. (b) Level scheme for single photon absorption. A two photon excitation, with coupling constants Ω_{sm} and Ω_{ex}, produces a single excitation in a Rydberg state $|a\rangle$ shared by the trapped atoms. From there it decays with an enhanced rate Γ_{sf} due to the SPP coupling to $|s\rangle$. The state $|b\rangle$ represents all outcomes where information is lost.

Most experiments and theory to date in quantum information focus on coherent coupling and explicitly try to avoid decoherence. However, in some cases, decoherence can aid in controlling and speeding up a desired quan-

tum dynamical process [10]. Controlled decoherence can, therefore, be a useful tool for designing quantum devices, e.g. to subtract single photons [5]. One of the challenges of using decoherence as a tool is to introduce the noise in a controlled way. One possibility that has been realized is to use a laser speckle field [5, 11], but this approach does not work for all applications. In our work, we introduce Rydberg atom SPP coupling [12] as a viable way to use decoherence in a controlled manner. Using the SPP coupling to a Rydberg atom allows dephasing to be controlled in many ways, including the distance dependence of the atom-SPP coupling, state selection, number of atoms making up a superatom and patterning of a surface with thin films to manipulate the SPP characteristics [13, 14]. More broadly, this hybrid quantum system offers the advantages of high frequency resonant coupling, the possibility of turning interactions on and off optically, terahertz coupling to conventional electronics and the ability to access ground atomic states with long coherence times. These properties can potentially be exploited to design other devices.

For our device, we envision atoms being confined in a trap close to an atom chip, $\sim 10\,\mu\text{m}$, which is covered with a dielectric, Figure 1. The trap volume is smaller than the Rydberg atom blockade volume, $\sim 1\,\mu\text{m}^3$. An electromagnetic field mode of a light source with Rabi frequency Ω_{sm} is focused through the atomic cloud. Together with a strong excitation laser, Ω_{ex}, the source drives a detuned two-photon excitation to a Rydberg state $|\text{a}\rangle$, with $\Delta_{\text{e}} \gg \Omega_{\text{ex}}$, where Δ_{e} is the detuning from an intermediate state $|\text{e}\rangle$. The single atom two photon Rabi frequency $\Omega_{\text{a}} = \Omega_{\text{sm}}\Omega_{\text{ex}}/(4\Delta_{\text{e}})$. Under these conditions, the effective Rabi frequency for this superatom state is $\Omega_{\text{eff}} = \sqrt{N}\Omega_{\text{a}}$ [9]. Since Δ_{e} is larger than Ω_{sm} and Ω_{ex}, the excitation linewidth is determined by Ω_{eff} and the decay rate of the Rydberg state. When the Rydberg atom blockade shifts are much greater than the effective linewidth, all other photons from the source are transmitted through the trap, Figure 2a. A series of traps along the propagation direction of the source mode allows for multiple subtractions and counting of photons.

For a practical device, the superatom excitation needs to be irreversibly transferred to a storage state $|\text{s}\rangle$ so that it decouples from the light fields and can be read out. It is important that this process happens as fast as possible with maximum efficiency, implying optimization occurs for critical damping. For critical damping, the decay rate to $|\text{s}\rangle$ is two times faster than the effective two-photon Rabi frequency, $\Gamma_{\text{sf}} = 2\Omega_{\text{eff}}$ [5], Figure 3. Reduction of the Rydberg blockade radius due to additional broadening associated with critical damping is small because of the long range dependence of the Rydberg atom interactions on internuclear separation, Figure 2a. The transfer probability and time depend on the distance between the atom cloud and the surface providing a variable to tune them, Figure 2b.

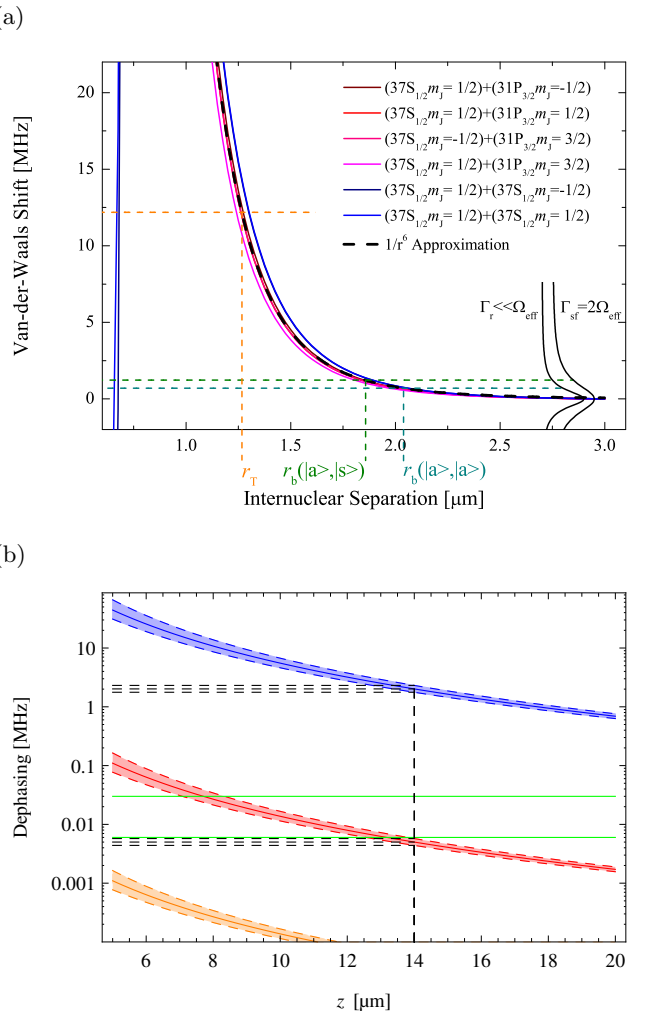

FIG. 2. (Color online) (a) Rydberg interaction and blockade radius for $(|\text{a}\rangle, |\text{a}\rangle) = (|37\text{S}_{1/2}\rangle, |37\text{S}_{1/2}\rangle)$ and $(|\text{a}\rangle, |\text{s}\rangle) = (|37\text{S}_{1/2}\rangle, |31\text{P}_{3/2}\rangle)$. The potentials are well approximated by a $1/r^6$ behavior. For this combination of states the C_6 coefficients are similar. The linewidth (dashed lines) for the unshifted Rydberg states for large distances are indicated, which defines blockade radii r_{b}. (b) LaF_3 induced dephasing rate for state $|\text{a}\rangle$ (blue) in resonance, (red) detuned by $2\,\text{cm}^{-1}$ from a polariton resonance at $40.8\,\text{cm}^{-1}$ with a width of $0.2\,\text{cm}^{-1}$ for a superatom consisting of 100 atoms and (orange) a single atom detuned by $2\,\text{cm}^{-1}$ in a $1.25\,\mu\text{m}$ diameter trap. The dashed lines mark the spread due to the finite size of the trap. The proposed trapping distance of $14\,\mu\text{m}$ is shown and the green lines indicate the natural decay rates of 6 kHz and 30 kHz used for simulations.

The excitation stored in $|\text{s}\rangle$ can be detected via the scheme described in [5, 15, 16]. In this method, the remaining ground state atoms are used to detect $|\text{s}\rangle$. The Rydberg interaction between $|\text{s}\rangle$ and another Rydberg state $|\text{d}\rangle \neq |\text{a}\rangle$ or $|\text{s}\rangle$ shifts $|\text{d}\rangle$ out of two photon resonance for a read out Rydberg atom EIT scheme [17, 18]. $|\text{d}\rangle$ changes the index of refraction for a probe beam associated with the readout EIT. The change in refractive

index can be detected by means of a homodyne measurement.

To demonstrate our approach, we chose $|\mathrm{a}\rangle$ and $|\mathrm{s}\rangle$ using several criteria. $|\mathrm{a}\rangle$ is coupled via a two photon transition from $|\mathrm{g}\rangle$, limiting us to nS and nD states for $|\mathrm{a}\rangle$, assuming alkali atoms. The transition dipole moment between $|\mathrm{a}\rangle$ and $|\mathrm{s}\rangle$ has to be strong enough to achieve sufficient coupling between the Rydberg state and the SPP. The constraint on the SPP coupling limits $|\mathrm{s}\rangle$ to n'P and n'F states, where $|n-n'|$ is small. To enforce decay, $|\mathrm{s}\rangle$ has to be lower in energy than $|\mathrm{a}\rangle$. The energy difference between $|\mathrm{a}\rangle$ and $|\mathrm{s}\rangle$ also has to be resonant with the SPP. For common materials, the frequency of the lowest SPP modes range from $\sim 40\,\mathrm{cm}^{-1}$ to $150\,\mathrm{cm}^{-1}$, e.g. LaF_3: $41\,\mathrm{cm}^{-1}$[19] and quartz: $128\,\mathrm{cm}^{-1}$[20]. $|\mathrm{s}\rangle$ should also be chosen so it does not couple to SPPs, but provides a large enough blockade radius to prevent further light absorption by the cloud. Finally, r_b has to be large enough to provide full blockade for trap sizes on the order of $1\,\mu\mathrm{m}^3$. r_b places a lower limit on n.

Given this set of constraints, we chose ^{87}Rb with $|\mathrm{a}\rangle = \left|37\mathrm{S}_{1/2}\right\rangle$ for our calculations. In contrast to D-states with similar n, S-states provide repulsive Rydberg atom interactions, so no molecules can be formed [21–23]. The transition energy to $|\mathrm{s}\rangle = \left|31\mathrm{P}_{3/2}\right\rangle$ is $\sim 40.8\,\mathrm{cm}^{-1}$, matching the lowest SPP of LaF_3. In general, the SPP modes of a material are tunable by changing the temperature and the orientation of the crystal surface. A $\sim 40.8\,\mathrm{cm}^{-1}$ SPP has a wavelength of $244\,\mu\mathrm{m}$ ensuring that the trap is in the near field regime for atom - surface separations of less than $\lambda/2\pi \approx 39\,\mu\mathrm{m}$.

Figure 2a shows a calculation of the energy shift as a function of internuclear separation [24, 25] for two atoms in $|\mathrm{a}\rangle$ (red colors) and one in $|\mathrm{a}\rangle$ and the other one in $|\mathrm{s}\rangle$ (blue colors). The plots show that for $|\mathrm{a}\rangle = \left|37\mathrm{S}_{1/2}\right\rangle$ and $|\mathrm{s}\rangle = \left|31\mathrm{P}_{3/2}\right\rangle$ the energy shift dependence on atom separation is almost the same in both cases. The blockade effect does not change significantly if the excitation decays from $|\mathrm{a}\rangle$ to $|\mathrm{s}\rangle$. For the internuclear separations shown, the actual potentials are well approximated by the r^{-6} dependence of a Van-der-Waals interaction.

On the lower right side of Figure 2a, the excitation linewidth for the cases when Ω_ex dominates, and when the decay is optimized, $\Gamma_\mathrm{sf} = 2\Omega_\mathrm{eff}$, are also shown. For these calculations, an experimentally feasible $\Omega_\mathrm{eff} = 2\pi \times 1\,\mathrm{MHz}$ [26] was used. By comparing these linewidths with the Van-der-Waals shift, r_b can be obtained. Once the shift is larger than the linewidth, the excitation is out of resonance with the light fields. r_b without coupling to the polaritons is [6–9]

$$r_\mathrm{b}(|\mathrm{a}\rangle, |\mathrm{s}\rangle) \approx \sqrt[6]{\frac{C_6(|\mathrm{a}\rangle, |\mathrm{s}\rangle)}{\hbar\sqrt{\Omega_\mathrm{eff}^2/2}}}, \tag{1}$$

but changes due to the shorter lifetime of $|\mathrm{a}\rangle$ and the different C_6 coefficient to

$$r_\mathrm{b}(|\mathrm{a}\rangle, |\mathrm{s}\rangle) \approx \sqrt[6]{\frac{C_6(|\mathrm{a}\rangle, |\mathrm{s}\rangle)}{\hbar\sqrt{(\Gamma_\mathrm{sf}/2)^2 + \Omega_\mathrm{eff}^2/2}}}. \tag{2}$$

after decay to $|\mathrm{s}\rangle$. The reduction of r_b due to optimization of the damping is as small as $r_\mathrm{b}(|\mathrm{a}\rangle, |\mathrm{s}\rangle)/r_\mathrm{b}(|\mathrm{a}\rangle, |\mathrm{a}\rangle) \approx \sqrt[12]{1/3} \approx 0.9$ for $\Gamma_\mathrm{sf} = 2\Omega_\mathrm{eff}$ and $C_6(|\mathrm{a}\rangle, |\mathrm{a}\rangle) \approx C_6(|\mathrm{a}\rangle, |\mathrm{s}\rangle)$. To strongly suppress a second excitation in the trap, the blockade shift has to be much larger than the excitation linewidth. $r_\mathrm{T} \approx 1.25\,\mu\mathrm{m}$ marks the distance at which the excitation probability drops below 1%. For further calculations this value will be used for the trap diameter.

To model the interaction between the Rydberg atom and SPP in the near field regime, we follow the approach in [27]. The transition dipole moment $\langle \mathrm{a}|\,\hat{d}\,|\mathrm{s}\rangle$ couples the excitation in $|\mathrm{a}\rangle$ to a SPP mode with frequency ω_pol and linewidth Γ_pol. Γ_pol results from decay of the SPP into bulk polariton modes. The Rydberg atom decay rate has a z^{-3} dependence, where z is the distance between the Rydberg atom and the surface:

$$\Gamma_\mathrm{sf} = \frac{\sigma^2}{8\pi\epsilon_0 h z^3}\left|\langle \mathrm{a}|\,\hat{d}\,|\mathrm{s}\rangle\right|^2 \frac{\omega_\mathrm{pol}^2\omega_{|\mathrm{a}\rangle,|\mathrm{s}\rangle}\Gamma_\mathrm{pol}}{\left(\omega_\mathrm{pol}^2 - \omega_{|\mathrm{a}\rangle,|\mathrm{s}\rangle}^2\right)^2 + \omega_{|\mathrm{a}\rangle,|\mathrm{s}\rangle}^2\Gamma_\mathrm{pol}^2}, \tag{3}$$

where $\sigma^2 = (\varepsilon_0 - 1)/(\varepsilon_0 + 1) - (\varepsilon_\infty - 1)/(\varepsilon_\infty + 1)$ is the difference in polarizability of the dielectric at low and high frequency. $\omega_{|\mathrm{a}\rangle,|\mathrm{s}\rangle}$ is the transition frequency between the states $|\mathrm{a}\rangle$ and $|\mathrm{s}\rangle$. The rate is enhanced at room temperature by a thermal factor $\Theta = (1 - \exp(-\beta\hbar\omega_\mathrm{pol}))^{-1} \approx 3$. If the SPP is resonant with the atomic transition, $\omega_{|\mathrm{a}\rangle,|\mathrm{s}\rangle} = \omega_\mathrm{pol}$, the Lorentzian in Equation (3) reduces to a resonant factor $\omega_\mathrm{pol}/\Gamma_\mathrm{pol}$, which can be more than 100. For example, the resonance in LaF_3 (quartz) at $41\,\mathrm{cm}^{-1}$ ($394\,\mathrm{cm}^{-1}$) has a relative width $\gamma = 0.005$ [19] ($\gamma = 0.007 \pm 0.001$ [20]) resulting in an resonant enhancement of $1/\gamma = 200$ ($1/\gamma \approx 143$). For a superatom, the transition dipole moment is also enhanced by a factor $\sqrt{N}$ resulting in a further increase of Γ_pol by N. The resonant coupling rate between the superatom and the SPP follows as

$$\Gamma_\mathrm{sf,opt} = \frac{\sigma^2 N\Theta}{8\pi\epsilon_0 h z^3}\left|d_\mathrm{single}\right|^2 \frac{\omega_\mathrm{pol}}{\Gamma_\mathrm{pol}}. \tag{4}$$

Figure 2b shows the decay rate (blue) for a superatom consisting of $N = 100$ atoms. A superatom of this size can be realized in magnetic microtraps with sub-Poissonian number fluctuations [28]. The single atom transition dipole moment $d_\mathrm{single} = \left\langle 37\mathrm{S}_{1/2}\right|\hat{d}\left|31\mathrm{P}_{3/2}\right\rangle \approx 15.5\,\mathrm{ea}_0$. The SPP is chosen to be resonant with $\omega_\mathrm{pol} = 40.8\,\mathrm{cm}^{-1}$ with $\Gamma_\mathrm{pol} = 0.2\,\mathrm{cm}^{-1}$, LaF_3. The dielectric constants for LaF_3 are $\varepsilon_0 = 14$ and $\varepsilon_\infty = 2.56$ [29]. For a distance $z \approx 14\,\mu\mathrm{m}$, $\Gamma_\mathrm{sf,opt} = 2\Omega_\mathrm{eff} \approx 2\pi \times 2\,\mathrm{MHz}$ is

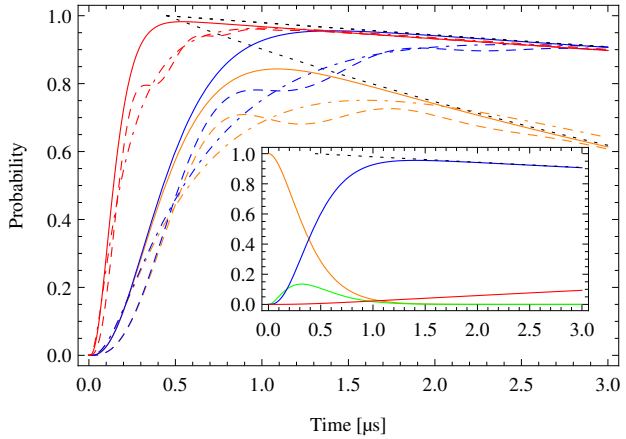

FIG. 3. (Color online) Probability of finding the system in $|s\rangle$ for different parameters. orange: $\Gamma_r = 2\pi \times 30\,\mathrm{kHz}$, $\Omega_{\mathrm{eff}} = 2\pi \times 1\,\mathrm{MHz}$, blue: $\Gamma_r = 2\pi \times 6\,\mathrm{kHz}$, $\Omega_{\mathrm{eff}} = 2\pi \times 1\,\mathrm{MHz}$, red: $\Gamma_r = 2\pi \times 6\,\mathrm{kHz}$, $\Omega_{\mathrm{eff}} = 2\pi \times 3\,\mathrm{MHz}$. The dashed line represents the underdamped case, $\Gamma_{sf} = \Omega_{\mathrm{eff}}/2$ and the dot-dashed line shows the overdamped regime, $\Gamma_{sf} = 4\Omega_{\mathrm{eff}}$. The solid line represents the crossover, $\Gamma_{sf} = 2\Omega_{\mathrm{eff}}$, where the transfer is the fastest. The dotted black lines indicate the Γ_r. Inset: Probability of finding the system in $|g\rangle$ (orange), $|a\rangle$ (green), $|s\rangle$ (blue) and $|b\rangle$ (red) for $\Omega_{\mathrm{eff}} = 2\pi \times 1\,\mathrm{Mhz}$, $\Gamma_{sf} = 2\Omega$, $\Gamma_r = 2\pi \times 6\,\mathrm{kHz}$.

achieved. $z \approx 14\,\mu\mathrm{m}$ is compatible with current trapping techniques [30].

After decay to $|s\rangle$, the coherence of the superatom, and therefore the N-enhancement, is lost. If $|s\rangle$ is detuned from the same or a similar SPP by $10\Gamma_{\mathrm{pol}}$ (orange), its decay is completely determined by $\Gamma_{r,37S_{1/2}} = 2\pi \times 6\,\mathrm{kHz}$ [31] and $\Gamma_{r,31P_{3/2}} = 2\pi \times 6.6\,\mathrm{kHz}$ [32]. A possible detection state $|d\rangle$, of which there are many possibilities, whose closest transition is also detuned by $10\Gamma_{\mathrm{pol}}$ (red), but still is in a coherent superposition, also couples to the surface at a rate comparable to Γ_r at the desired distance.

To simulate the system dynamics, we used a density matrix approach for the level scheme shown in Figure 1b. We adiabatically eliminated $|e\rangle$ due to the large detuning $\Delta_e \gg \Omega_{\mathrm{ex}}$ and used Ω_{eff} to coherently couple $|g\rangle$ and $|a\rangle$. The decay from $|a\rangle$ into $|s\rangle$ is modeled as an enhanced spontaneous decay with a rate Γ_{sf}. Both Rydberg states $|a\rangle$ and $|s\rangle$ decay with the Rydberg decay rate Γ_r into $|b\rangle$. $|b\rangle$ models the loss in the overall system dynamics.

Figure 3 shows the result of the calculations for $\Omega_{\mathrm{eff}} = 2\pi \times 1\,\mathrm{MHz}$ (blue). The solid line represents the dynamics for the optimized decay rate $\Gamma_{sf} = 2\Omega_{\mathrm{eff}}$. In this case, the transfer to $|s\rangle$ is the fastest and the readout time is only limited by the Rydberg decay. Our results indicate a readout window of more than $2\,\mu\mathrm{s}$ is available with a fidelity $f > 90\%$. The transfer is slower for the over- and underdamped regime (dot-dashed and dashed line), but $f = 90\%$ can still be achieved, albeit in a shorter time window. f strongly depends on the Rydberg lifetime. For $\Gamma_r = 2\pi \times 30\,\mathrm{kHz}$ instead of $2\pi \times 6\,\mathrm{kHz}$, the time window for $f > 80\%$ is decreased to $< 1\,\mu\mathrm{s}$. The performance of the system can be improved with faster dynamics. The red line shows the case for an effective Rabi frequency $\Omega_{\mathrm{eff}} = 2\pi \times 3\,\mathrm{MHz}$.

We have shown that the coupling between a Rydberg state and a SPP can be used to add decoherence in a controlled way to make a quantum device, a single photon counter or subtractor. The parameters discussed in the text are all experimentally achievable. The process can be sped up by trapping the atoms closer to the surface or utilizing stronger, perhaps optimally engineered [33], Rydberg atom-SPP coupling. Trapping atoms closer to the surface increases the spatial spread of Rydberg atom-SPP coupling rates which has to be compensated for by smaller trap sizes. Perhaps more significantly, we have introduced a new hybrid quantum system that can be further investigated for other quantum device applications now that it has been shown promising. The Rydberg atom- SPP hybrid quantum system is particularly interesting because of the spectral range where the couplings between the SPP and Rydberg atom lie, $\sim 1\,\mathrm{THz}$. We are currently investigating the couplings between Rydberg atoms and SPP's experimentally using optical measurement techniques we have developed for absolute electric field measurement [34, 35].

We thank G. Agarwal and T. Pfau for useful discussions. This work was supported by the NSF (PHY-1104424).

* h.kuebler@physik.uni-stuttgart.de
† shaffer@nhn.ou.edu

[1] R. Schoelkopf and S. Girvin, Nature **451**, 664 (2008).
[2] J. P. Shaffer, Nat. Phot. **5**, 451 (2011).
[3] A. Anderson, S. Haroche, E. A. Hinds, W. Jhe, and D. Meschede, Phys. Rev. A **37**, 3594 (1988).
[4] H. Failache, S. Saltiel, A. Fischer, D. Bloch, and M. Ducloy, Phys. Rev. Lett. **88**, 243603 (2002).
[5] J. Honer, R. Löw, H. Weimer, T. Pfau, and H. P. Büchler, Phys. Rev. Lett. **107**, 093601 (2011).
[6] D. Tong, S. M. Farooqi, J. Stanojevic, S. Krishnan, Y. P. Zhang, R. Côté, E. E. Eyler, and P. L. Gould, Phys. Rev. Lett. **93**, 063001 (2004).
[7] T. C. Liebisch, A. Reinhard, P. R. Berman, and G. Raithel, Phys. Rev. Lett. **95**, 253002 (2005).
[8] K. Singer, M. Reetz-Lamour, T. Amthor, L. G. Marcassa, and M. Weidemüller, Phys. Rev. Lett. **93**, 163001 (2004).
[9] R. Heidemann, U. Raitzsch, V. Bendkowsky, B. Butscher, R. Löw, L. Santos, and T. Pfau, Phys. Rev. Lett. **99**, 163601 (2007).
[10] M. B. Plenio and H. S. F., New J. Phys. **10**, 113019 (2008).
[11] J. Billy, V. Josse, Z. Zuo, A. Bernard, B. Hambrecht, P. Lugan, D. Clement, L. Sanchez-Palencia, P. Bouyer, and A. Aspect, Nature **453**, 891 (2008).
[12] H. Kübler, J. Shaffer, T. Baluktsian, R. Löw, and T. Pfau, Nat. Phot. **4**, 112 (2010).

[13] V. Agranovich and D. Mills, *Surface Polaritons: Electromagnetic Waves at Surfaces and Interfaces, Volume 1*, Modern Problems in Condensed Matter Sciences (North Holland, 1982).

[14] A. Kamli, S. A. Moiseev, and B. C. Sanders, Phys. Rev. Lett. **101**, 263601 (2008).

[15] M. Müller, I. Lesanovsky, H. Weimer, H. P. Büchler, and P. Zoller, Phys. Rev. Lett. **102**, 170502 (2009).

[16] M. Saffman and K. Mølmer, Phys. Rev. Lett. **102**, 240502 (2009).

[17] M. Fleischhauer, A. Imamoglu, and J. P. Marangos, Rev. Mod. Phys. **77**, 633 (2005).

[18] A. K. Mohapatra, T. R. Jackson, and C. S. Adams, Phys. Rev. Lett. **98**, 113003 (2007).

[19] R. S. Meltzer, J. E. Rives, and G. S. Dixon, Phys. Rev. B **28**, 4786 (1983).

[20] W. G. Spitzer and D. A. Kleinman, Phys. Rev. **121**, 1324 (1961).

[21] A. Schwettmann, K. R. Overstreet, J. Tallant, and J. P. Shaffer, J. Mod. Opt. **54**, 2551 (2007).

[22] K. R. Overstreet, A. Schwettmann, J. Tallant, and J. P. Shaffer, Phys. Rev. A **76**, 011403 (2007).

[23] K. R. Overstreet, A. Schwettmann, J. Tallant, D. Booth, and J. P. Shaffer, Nat. Phys. **5**, 581 (2009).

[24] A. Schwettmann, J. Crawford, K. R. Overstreet, and J. P. Shaffer, Phys. Rev. A **74**, 020701 (2006).

[25] J. S. Cabral, J. M. Kondo, L. F. Gonçalves, V. A. Nascimento, L. G. Marcassa, D. Booth, J. Tallant, A. Schwettmann, K. R. Overstreet, J. Sedlacek, and J. P. Shaffer, J. Phys. B **44**, 184007 (2011).

[26] E. Urban, T. A. Johnson, T. Henage, L. Isenhower, D. D. Yavuz, T. G. Walker, and M. Saffman, Nat. Phys. **5**, 110 (2009).

[27] G. Barton, Proc. R. Soc. A **453**, 2461 (1997).

[28] S. Whitlock, C. F. Ockeloen, and R. J. C. Spreeuw, Phys. Rev. Lett. **104**, 120402 (2010).

[29] J. R. Igel, M. C. Wintersgill, J. J. Fontanella, A. V. Chadwick, C. G. Andeen, and V. E. Bean, J. Phys. C **15**, 7215 (1982).

[30] V. Leung, A. Tauschinsky, N. Druten, and R. Spreeuw, Quant. Inf. Proc. **10**, 955 (2011).

[31] D. B. Branden, T. Juhasz, T. Mahlokozera, C. Vesa, R. O. Wilson, M. Zheng, A. Kortyna, and D. A. Tate, J. Phys. B **43**, 015002 (2010).

[32] I. I. Beterov, I. I. Ryabtsev, D. B. Tretyakov, and V. M. Entin, Phys. Rev. A **79**, 052504 (2009).

[33] N. Dahan, A. Niv, G. Biener, V. Kleiner, and E. Hasman, Appl. Phys. Lett. **86**, 191102 (2005).

[34] J. A. Sedlacek, A. Schwettmann, H. Kübler, R. Löw, T. Pfau, and J. P. Shaffer, Nat. Phys. **8**, 819 (2012).

[35] J. A. Sedlacek, , H. Kübler, A. Schwettmann, and J. P. Shaffer, `arXiv:1304.4299[physics.atom-ph]`.